LASER INTERFEROMETER GRAVITATIONAL WAVE OBSERVATORY
- LIGO -
CALIFORNIA INSTITUTE OF TECHNOLOGY
MASSACHUSETTS INSTITUTE OF TECHNOLOGY

Technical Note	LIGO-T980044-A	-E	98.05.20
Document	*Doc Number*	*Group*	*Date*

Determination of Global and Local Coordinate Axes for the LIGO Sites

Title

William Althouse
Larry Jones
Albert Lazzarini

Author[s]

This is an internal working note of
the LIGO Project

California Institute of Technology
LIGO Project - MS 18-33
Pasadena CA 91125
Phone +1.626.395.2966
Fax +1.626.304.9834
E-mail: info@ligo.caltech.edu

Massachusetts Institute of Technology
LIGO Project - MS 20B-145
Cambridge, MA 01239
Phone +1.617.253.4824
Fax +1.617.253.7014
E-mail: info@ligo.mit.edu

WWW: http://www.ligo.caltech.edu

Table of Contents

1 Purpose 3
2 Hanford Survey Data 4
 2.1 Fit to the Survey Data 6
 2.2 Error propagators in the fits 11
 2.3 Hanford Local Coordinate Systems in each station 15
3 Livingston Survey Data 16
4 Graphical representations of the interferometer planes for each site 16

List of Figures

Figure 1: Geodetic and Earth-Fixed Coordinates 7
Figure 2: Scatter plots of fit residuals in plane normal to global axis. 10
Figure 3: Dependence of residuals on distance along the arms 10
Figure 4: Pitch, yaw, and roll axes for the orientation error analysis. 11
Figure 5: Representation of the interferometer plane inclinations at the two LIGO sites. 17

List of Tables

Table 1: Relevant, Previously Released LIGO Documents 3
Table 2: Design values of the global coordinate positions of BT/VE interface markers 4
Table 3: Cardinal Marker Survey Data 5
Table 4: Parameters resulting from best fit to the survey data 8
Table 5: Global coordinate positions of as-built BT/VE interface markers 9
Table 6: Sensitivity matrix for the XG coordinate for BTVE markers 12
Table 7: Sensitivity matrix for the YG coordinate for BTVE markers 13
Table 8: Sensitivity matrix for the ZG coordinate for BTVE markers 14
Table 9: Uncertainties in fitted parameters. Changing the best fit values by these amounts result in a doubling of the RMS residual fitting error. 15
Table 10: Hanford Vertex Global-Local System Direction Cosines 15
Table 11: Hanford X End Station (d= 4000m) Global-Local System Direction Cosines 15
Table 12: Hanford Y End Station (d= 4000m) Global-Local System Direction Cosines 16
Table 13: Hanford X Mid-Station (d = 2000m) Global-Local System Direction Cosines 16
Table 14: Hanford Y Mid-Station (d = 2000m) Global-Local System Direction Cosines 16

1 PURPOSE

This document uses survey data taken during the course of fabricating the beam tubes at the LIGO Hanford Observatory (LHO) to determine the as-built orientation and origin for the LIGO Site Coordinate Axes.

Table 1 lists previously issued documents that contain relevant information. The present document supersedes previously released determinations of the coordinate axes because more information is now known about the as-built beam tube and marker geometry. Some earlier analyses used a spherical earth model. At that time, the rough data that were available could be adequately described; later, higher precision GPS data dictated switching to the accepted WGS-84 ellipsoidal model of the earth for refined analyses.

Table 1: Relevant, Previously Released LIGO Documents

LIGO Document umber	*Title*	*Description*
L950128	LIGO Coordinate System	Gives an operational definition of the site global and local coordinate axes
T950004	Derivation of Global and Local Coordinate Axes for the LIGO Sites	Takes the operational definition and derives the *design* beam centerline direction cosines, global and local coordinate axes. <u>Uses a spherical model for the earth and Parsons-provided rough grading survey data.</u>
T950107	Orientation of the LIGO Beam Center Lines with respect to foundation slabs	Written for PSI (the VE contractor) to document the angular deviation from local horizontal of the *design* beam tube centerlines in each of the LIGO stations. <u>Uses data appearing in</u> T950004 (i.e. spherical earth model).
T960176	Determination of the LIGO Global Coordinate Axes for Hanford, WA: final analysis of the LIGO BT/VE interface survey monuments.	Reports the results to a first best-fit determination of the plane defined by the eight cardinal points for the Hanford site. Uses early survey data from RSI and IMTEC. Results are superseded by present, more thorough, document.
D950021	LIGO Arm Layout	Drawing showing BT/VE interface locations
C962080	TDM 014C to CB&I	Provides the height offsets above the marker elevations for establishing the beam tube centerlines.

2 HANFORD SURVEY DATA

In the course of laying out the Hanford site, eight cardinal points were surveyed in preparation for fabrication and alignment of the beam tubes. These points defined the interface positions for the beam tube (BT) and vacuum equipment (VE) contracts. These points are identified by suitably inscribed marks on each of eight brass markers, denoted {BT/VE1, ..., BT/VE8} (see D950021 for specifications). The design positions in global coordinates of the interface markers are given in Table 2.

Table 2: Design values of the global coordinate positions of BT/VE interface markers

Marker ID	X_G	Y_G	Z_G
BT/VE 1	0.000	46.000	-1.070[a]
BT/VE 2	0.000	2007.500	-1.070
BT/VE 3	0.000	2027.000	-1.070
BT/VE 4	0.000	3988.500	-1.070
BT/VE 5	46.000	0.000	-1.070
BT/VE 6	2007.500	0.000	-1.070
BT/VE 7	2027.000	0.000	-1.070
BT/VE 8	3988.500	0.000	-1.070

a. The design for the BT centerline was to be 1.070 m above the finished slab.

BT/VE1 - BT/VE4 lie along the Y arm and BT/VE5 - BT/VE8 are similarly arranged along the X arm.

During the course of constructing the beam tubes, the markers were surveyed a number of times by different parties. Sometimes only a subset of the full three-dimensional position of the markers were determined (e.g., height only). In making use of all data, missing information has been substituted using complementary information from other surveys (e.g., height-only data were augmented with $\{\phi, \lambda\}$ data from other measurements). This will tend to artificially tighten the scatter in the those coordinate directions which are affected by the repeated use of the same $\{\phi, \lambda\}$ coordinates; however, this approach allows all height data to be used. This is desirable because height determinations were typically the noisiest and having more measurements serves to improve the level of precision of the dataset as a whole.

Table 2 presents the survey results for the eight BT/VE markers. The markers were placed on the as-built beam tube slabs. Their heights are affected by slight irregularities in the slab finish. After the first survey by IMTEC and RSI, LIGO determined the best estimate (at that time) for the vertical offsets above each of the markers where the beam tube centerline should be located. The last column in the table shows these vertical offsets. The global coordinate axes were determined by fitting to a beam tube centerline going through points at the indicated offsets above the markers. In reporting the marker locations, the offsets were then subtracted from the residuals to the fit in order to refer the monument locations on the slab surfaces.

Table 3: Cardinal Marker Survey Data

Marker ID *Source*	*Latitude*			*Longitude*			*Ellipsoidal height of marker*	*Design height of beam centerline above marker elevation*
	°	′	″	°	′	″	*m*	*m*
BT/VE1								
IMTEC RSI-GroundLoop RSI-GPS CBI-GPS (all same)	46	27	17.65230	-119	24	29.30959	141.4980	1.0602
BT/VE2								
IMTEC	46	26	40.30783	-119	25	43.65422	141.8340	1.0612
RSI-Ground Loop	46	26	40.30785	-119	25	43.65410	141.8260	1.0612
RSI-GPS	46	26	40.30785	-119	25	43.65410	141.8270	1.0612
CBI-GPS	46	26	40.30783	-119	25	43.65421	141.8390	1.0612
BT/VE3								
IMTEC	46	26	39.93653	-119	25	44.39319	141.8402	1.0612
RSI-Ground Loop	46	26	39.93649	-119	25	44.39314	141.8342	1.0612
RSI-GPS	46	26	39.93649	-119	25	44.39314	141.8310	1.0612
CBI-GPS	46	26	39.93653	-119	25	44.39319	141.8450	1.0612

Table 3: Cardinal Marker Survey Data

Marker ID *Source*	*Latitude*			*Longitude*			*Ellipsoidal height of marker*	*Design height of beam centerline above marker elevation*
	°	′	″	°	′	″	*m*	*m*
BT/VE4								
IMTEC	46	26	2.57842	-119	26	58.70927	142.7882	1.0592
RSI-Ground Loop	46	26	2.57842	-119	26	58.70928	142.7932	1.0592
RSI-GPS	46	26	2.57842	-119	26	58.70928	142.7980	1.0592
CBI-GPS	46	26	2.57842	-119	26	58.70928	142.7980	1.0592
BT/VE5								
IMTEC	46	27	19.73298	-119	24	28.83263	141.4677	1.0612
RSI-Ground Loop	46	27	19.73310	-119	24	28.83270	141.4677	1.0612
RSI-GPS	46	27	19.73310	-119	24	28.83270	141.4690	1.0612
CBI-GPS	46	27	19.73298	-119	24	28.83263	141.4650	1.0612
BT/VE6								
IMTEC	46	28	11.12085	-119	25	22.87130	140.5684	1.0569
RSI-Ground Loop	46	28	11.12114	-119	25	22.87150	140.5714	1.0569
RSI-GPS	46	28	11.12114	-119	25	22.87150	140.5650	1.0569
BT/VE7								
IMTEC	46	28	11.63174	-119	25	23.40854	140.5626	1.0579
RSI-Ground Loop	46	28	11.63199	-119	25	23.40886	140.5686	1.0579
RSI-GPS	46	28	11.63199	-119	25	23.40886	140.5600	1.0579
BT/VE8								
IMTEC	46	29	3.01234	-119	26	17.47572	140.2633	1.0632
RSI-Ground Loop	46	29	3.01263	-119	26	17.47612	140.2763	1.0632
RSI-GPS	46	29	3.01263	-119	26	17.47612	140.2640	1.0632
CBI-GPS	46	29	3.01234	-119	26	17.47572	140.2680	1.0632

2.1 Fit to the Survey Data

A *global orthonormal coordinate system* was determined which has its $\hat{x}_G$ and $\hat{y}_G$ axes along best fit lines defined by the markers along the arms. The $\hat{z}_G$ axis is defined by the cross product:

$\hat{z}_G = \hat{x}_G \times \hat{y}_G$.

The data of Table 3 were converted to the earth-fixed Cartesian system, $\{\hat{x}_E, \hat{y}_E, \hat{z}_E\}$, used for geodetic work. In this system, $\hat{x}_E$ pierces the earth surface at $\{\phi, \lambda\}$ = {000, 000}, $\hat{y}_E$ pierces the earth's surface at $\{\phi, \lambda\}$ = {000, 090E}, and $\hat{z}_E$ pierces the earth's surface at $\{\phi, \lambda\}$ = {090N, 000}. The relationship between the coordinates of a point $\{h, \phi, \lambda\}$ and $\{X_E, Y_E, Z_E\}$ is depicted in Figure 1.

Figure 1: Geodetic and Earth-Fixed Coordinates

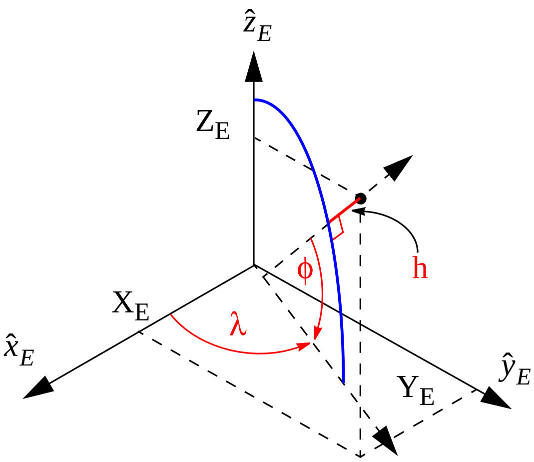

The functional relationships are given by:

$$X_E = ((R[\phi] + h)Cos\phi Cos\lambda$$

$$Y_E = (R[\phi] + h)Cos\phi Sin\lambda$$

$$Z_E = ([1 - \varepsilon^2]R[\phi] + h)Sin\phi$$

The earth model WGS-84, is described by an oblate ellipsoid with its semi-minor axis, b = 6356752.314 m, along $\hat{z}_E$, semi-major axis with value a = 6378137 m, and eccentricity giving $[1 - \varepsilon^2]$ = 0.993306. $R[\phi]$ is the local radius of curvature of the ellipsoid at latitude ϕ:

$$R[\phi] = \frac{a^2}{a^2 Cos^2\phi + b^2 Sin^2\phi}$$

Note that in the geodetic model the vector h is aligned along the local surface normal. Consequently its extension to the equatorial plane does not, in general, intersect the origin.

The set of orthonormal axes which best describes the Cartesian data for the markers were determined by a χ^2 minimization of the transverse (2D) residuals of the marker positions from the best-fit axes. There are six degrees of freedom for the fit: 3 translational and three rotational. These were chosen as:

- **three** coordinates for the vertex, $\{X_v, Y_v, Z_v\}$;

- **two** direction cosines for one axis, $\{n_{xx}, n_{xy}, 1\}$; the z component was fixed.
- **one** direction cosine for the remaining axis (the orientation of the remaining axis in the plane normal to the first axis), $\left\{n_{yx}, \frac{-(n_{xx}n_{yx}+1)}{n_{xy}}, 1\right\}$; this is done by fitting the x component of the second normal, constraining the y and z components.

The errors associated with many of the measured data were not reported in the surveys. Therefore the fitting procedure assumed equal weights for all data: the χ^2 optimization was reduced to a least squares minimization.

The 3-axis RMS residual for the best fit was 0.0053 m. This fit gives parameter values listed in Table 4.

Table 4: Parameters resulting from best fit to the survey data

Parameter	*Value*	*Estimated Error*	*Units*
Vertex	Global $\{\hat{x}_G, \hat{y}_G, \hat{z}_G\}$: {0,0,0}	{0.0064, 0.0073, 0.0050}	m
	Geodetic $\{h, \phi, \lambda\}$:{142.554,{46,27,18.528},{-119,24,27.5657}}	-	m
	Earth-fixed $\{\hat{x}_E, \hat{y}_E, \hat{z}_E\}$: {-2.1614149 10^6, -3.8346952 10^6, 4.6003502 10^6}	{0.0066, 0.0057, 0.0054}	m
$\hat{x}_G$	Global $\{\hat{x}_G, \hat{y}_G, \hat{z}_G\}$: {1,0,0}	-	
	Earth-fixed $\{\hat{x}_E, \hat{y}_E, \hat{z}_E\}$: {-0.223892, 0.799831, 0.556905}	-	
	Compass Direction: N35.9994° W (ref. geodetic north)[a]	1.93 10^{-6}	radian
	Angle relative to local horizontal at Vertex: -6.195 10^{-4}	2.73 10^{-6}	radian
$\hat{y}_G$	Global $\{\hat{x}_G, \hat{y}_G, \hat{z}_G\}$: {0,1,0}		
	Earth-fixed $\{\hat{x}_E, \hat{y}_E, \hat{z}_E\}$: {-0.913978, 0.0260945, -0.404923}		
	Compass Direction: S54.0006° W (see footnote a)	1.93 10^{-6}	radian
	Angle relative to local horizontal at Vertex: -1.25 10^{-5}	2.73 10^{-6}	radian
$\hat{z}_G$	Global $\{\hat{x}_G, \hat{y}_G, \hat{z}_G\}$: {0,0,1}		
	Earth-fixed $\{\hat{x}_E, \hat{y}_E, \hat{z}_E\}$: {-0.338402,-0.599658,0.725186}		
	Deviation from zenith at vertex: 6.195 10^{-4}, toward $\hat{x}_G$	2.73 10^{-6}	radian

a. Site drawings call for arms to run N36.8° W and S53.2° W; these are referred to the WA state plane coordinates (northing & easting). Geodetic north is 47’39” (~0.8 °) W of grid north at the vertex.

Location of as-built BT/VE markers relative to global coordinate system

Using the coordinate system described above, the positions for each of the 8 BT/VE interface markers were determined by averaging the residuals from multiple measurements of individual markers. Table 5 presents the results.

Table 5: Global coordinate positions of as-built BT/VE interface markers

Marker ID	X_G	Y_G	Z_G
BT/VE 1	0.0000	46.0020	-1.0572
BT/VE 2	-0.0011	2007.5000	-1.0639
BT/VE 3	-0.00052	2027.0000	-1.0642
BT/VE 4	-0.0012	3988.5000	-1.0564
BT/VE 5	45.9970	0.0028	-1.0588
BT/VE 6	2007.5000	0.0010	-1.0585
BT/VE 7	2027.0000	-0.0004	-1.0571
BT/VE 8	3988.5000	-0.0023	-1.0630

The scatter of the residuals is presented graphically in Figures 2 and 3. Figure 2 presents the scatter in the plane normal to the axis for each arm. There is an apparent greater right-left scatter along the X arm. This is a result of the fact that the best description of the marker positions corresponds to two axes which are not exactly orthogonal: an optimization without imposing the orthogonality constraint between the best fit lines results in axes having an included angle ~ 1.3 microradians greater than 90 degrees. This fact may be seen in the lower panels of Figure 3 which present residuals in the horizontal plane as a function of their position along the arms.

Figure 2: Scatter plots of fit residuals in plane normal to global axis.

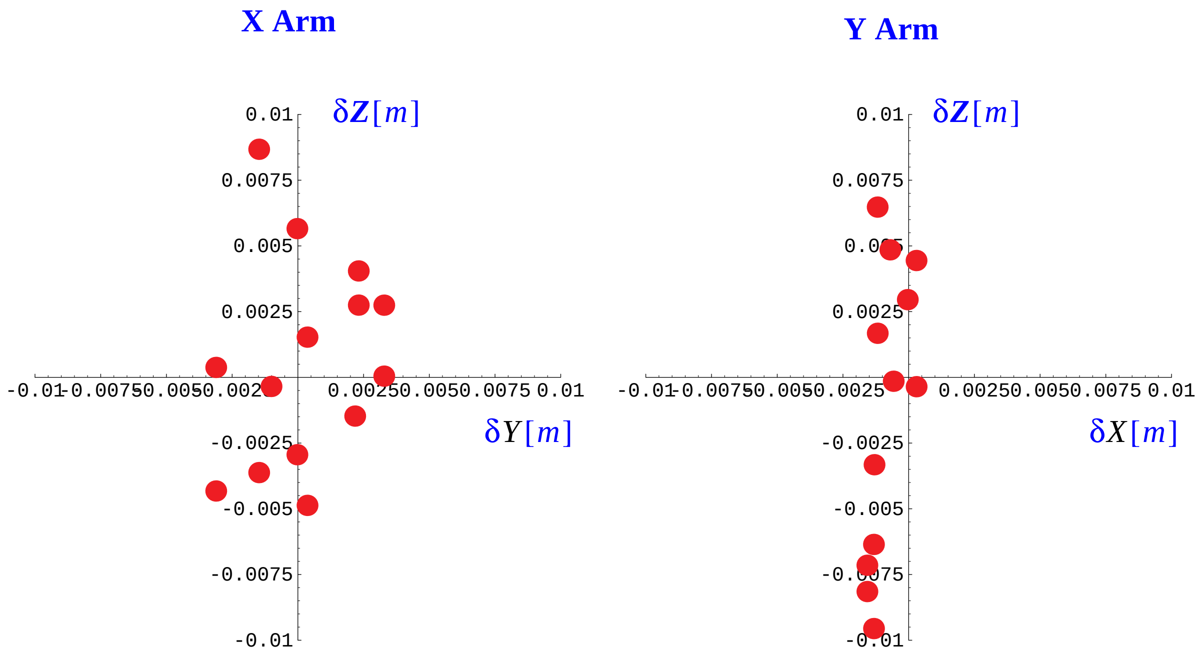

Figure 3: Dependence of residuals on distance along the arms.

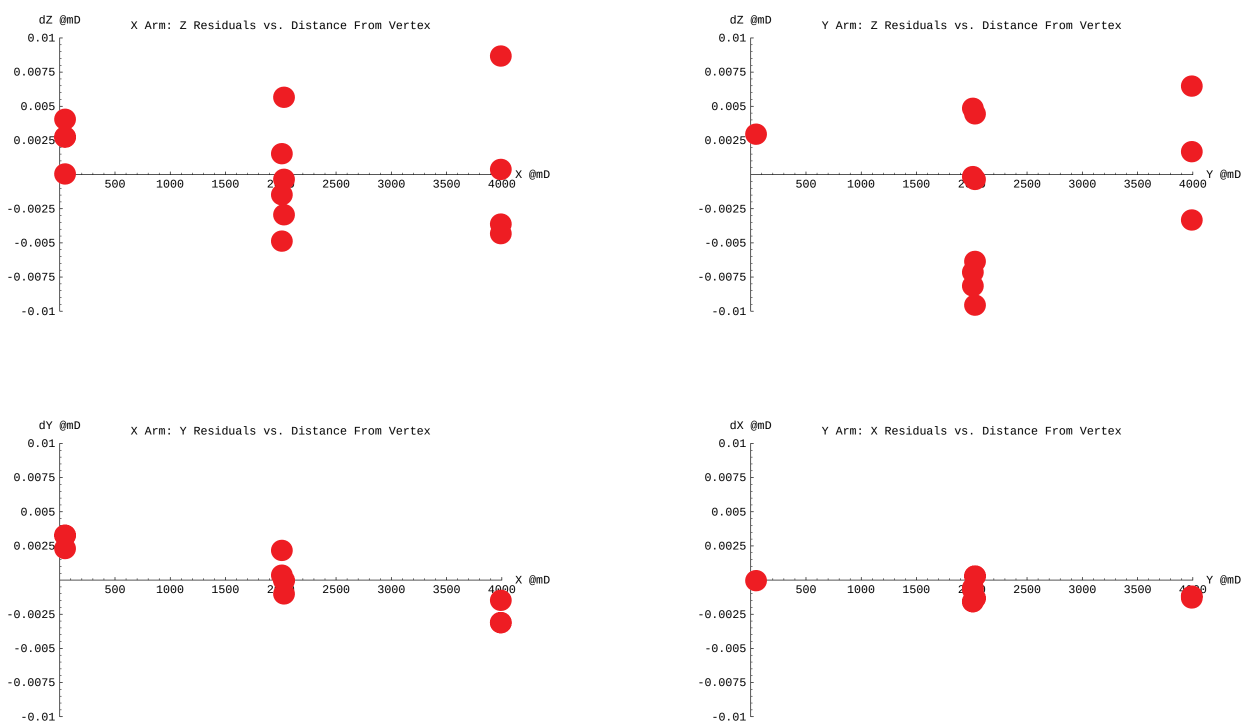

2.2 Error propagators in the fits

Any error in the estimated position of the vertex results in a common mode offset to all marker positions; errors in the estimated directions of the coordinate axis result in either differential mode or common mode offsets according which orientation angle is in error and the effect on marker position is in proportion to marker distances from the vertex. This behavior is represented by the error propagation matrices presented as Tables 6 - 8. Each table corresponds to one coordinate. The rows give the effects of parameter variations the eight marker locations. Vertex translational errors are referred along the global axes. Angular errors in the orientation of the axes are referred to roll, pitch and yaw of the $\hat{z}_G$ axis. Pitch gives a common mode up/down displacement for all markers. This rotation is denoted by θ_{CM} which arises from infinitesimal rotational errors about the axis

$$\hat{n}_{CM} = \frac{\hat{y}_G - \hat{x}_G}{\sqrt{2}} \quad ;$$

Yaw gives a differential mode up/down displacement for all markers. This rotation is denoted by θ_{DM} which arises from infinitesimal rotational errors about the axis

$$\hat{n}_{DM} = \frac{\hat{y}_G + \hat{x}_G}{\sqrt{2}}$$

θ_z corresponds to an error in marker positions which arises from infinitesimal rotational errors about the axis $\hat{z}_G$. The roll pitch and yaw axes are depicted in Figure 4.

Figure 4: Pitch, yaw, and roll axes for the orientation error analysis.

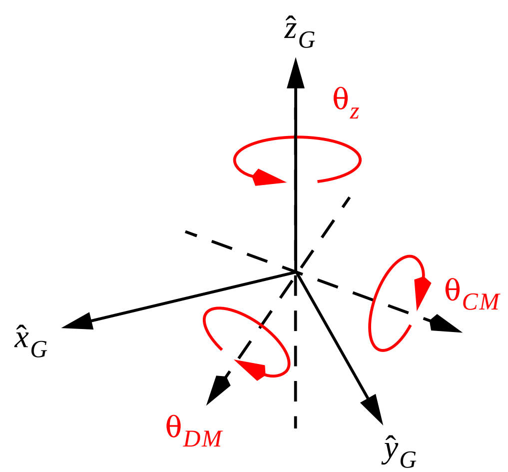

Table 6: Sensitivity matrix for the X_G coordinate for BTVE markers

Marker ID	$\frac{\partial}{\partial V_x}$ [m/m]	$\frac{\partial}{\partial V_y}$ [m/m]	$\frac{\partial}{\partial V_z}$ [m/m]	$\frac{\partial}{\partial \theta_{CM}}$ [m/rad]	$\frac{\partial}{\partial \theta_{DM}}$ [m/rad]	$\frac{\partial}{\partial \theta_z}$ [m/rad]
$BTVE1_x$	-0.224	0.800	0.557	-0.002091	-0.002091	46.002
$BTVE2_x$	-0.224	0.800	0.557	, 0.001873	0.001873	2007.502
$BTVE3_x$	-0.224	0.800	0.557	, 0.002090	0.002090	2027.003
$BTVE4_x$	-0.224	0.800	0.557	-0.001999	-0.001999	3988.504
$BTVE5_x$	-0.224	0.800	0.557	-0.001695	-0.001695	0.00279
$BTVE6_x$	-0.224	0.800	0.557	, 0.001135	0.001135	0.000963
$BTVE7_x$	-0.224	0.800	0.557	-0.0005588	-0.0005588	-0.000356
$BTVE8_x$	-0.224	0.800	0.557	-0.0001960	-0.0001960	-0.00230

Table 7: Sensitivity matrix for the Y_G coordinate for BTVE markers

Marker ID	$\frac{\partial}{\partial V_x}$ [m/m]	$\frac{\partial}{\partial V_y}$ [m/m]	$\frac{\partial}{\partial V_z}$ [m/m]	$\frac{\partial}{\partial \theta_{CM}}$ [m/rad]	$\frac{\partial}{\partial \theta_{DM}}$ [m/rad]	$\frac{\partial}{\partial \theta_z}$ [m/rad]
$BTVE1_y$	-0.914	0.0261	-0.405	-0.002091	0.002091	0.0000426
$BTVE2_y$	-0.914	0.0261	-0.405	0.001873	-0.001873	0.00111
$BTVE3_y$	-0.914	0.0261	-0.405	0.002090	-0.002090	0.000519
$BTVE4_y$	-0.914	0.0261	-0.405	-0.001999	0.001999	0.001217
$BTVE5_y$	-0.914	0.0261	-0.405	-0.001695	0.001695	-45.997
$BTVE6_y$	-0.914	0.0261	-0.405	0.001135	-0.001135	-2007.500
$BTVE7_y$	-0.914	0.0261	-0.405	-0.0005588	0.0005588	-2027.000
$BTVE8_y$	-0.914	0.0261	-0.405	-0.0001960	0.0001960	-3988.497

Table 8: Sensitivity matrix for the Z_G coordinate for BTVE markers

Marker ID	$\frac{\partial}{\partial V_x}$ [m/m]	$\frac{\partial}{\partial V_y}$ [m/m]	$\frac{\partial}{\partial V_z}$ [m/m]	$\frac{\partial}{\partial \theta_{CM}}$ [m/rad]	$\frac{\partial}{\partial \theta_{DM}}$ [m/rad]	$\frac{\partial}{\partial \theta_z}$ [m/rad]
$BTVE1_z$	-0.338	-0.600	0.725	32.528	-32.528	0
$BTVE2_z$	-0.338	-0.600	0.725	1419.517	-1419.519	0
$BTVE3_z$	-0.338	-0.600	0.725	1433.307	-1433.308	0
$BTVE4_z$	-0.338	-0.600	0.725	2820.298	-2820.299	0
$BTVE5_z$	-0.338	-0.600	0.725	32.527	32.523	0
$BTVE6_z$	-0.338	-0.600	0.725	1419.517	1419.516	0
$BTVE7_z$	-0.338	-0.600	0.725	1433.305	1433.306	0
$BTVE8_z$	-0.338	-0.600	0.725	2820.291	2820.295	0

Table 9 presents uncertainties in vertex position and axis orientations. The uncertainties were defined as the amount of parameter variation which results in a doubling of the RMS residuals from the minimum value 0.0053 m. The vector in Table 9 may be multiplied by each of the previous tables to obtain the (correlated) errors in marker positions.

Table 9: Uncertainties in fitted parameters. Changing the best fit values by these amounts result in a doubling of the RMS residual fitting error.

Parameter	Error
V_x	0.0064 m
V_x	0.0073 m
V_x	0.0050 m
θ_{CM}	2.73 10^{-6} rad
θ_{DM}	2.73 10^{-6} rad
θ_z	1.93 10^{-6} rad

2.3 Hanford Local Coordinate Systems in each station

Tables 10 - 14 present the direction cosines between the global coordinate system and the local coordinate systems for each station. The local coordinates are defined in LIGO-L950128 and LIGO-T950004 listed in Table 1.

Table 10: Hanford Vertex Global-Local System Direction Cosines

	$\hat{x}_L$	$\hat{y}_L$	$\hat{z}_L$
$\hat{x}_G$	1 - 1.91886e-7	7.7333e-9	-0.00061949
$\hat{y}_G$	7.7333e-9	1 - 7.7916e-11	0.0000124832
$\hat{z}_G$	0.00061949	-0.0000124832	1 - 1.91964e-7

Table 11: Hanford X End Station (d= 4000m) Global-Local System Direction Cosines

	$\hat{x}_L$	$\hat{y}_L$	$\hat{z}_L$
$\hat{x}_G$	1 - 3.07241e-11	0	7.8389e-6
$\hat{y}_G$	0	1 - 6.6491e-11	0.0000115318
$\hat{z}_G$	-7.8389e-6	-0.0000115318	1 - 9.7215e-11

Table 12: Hanford Y End Station (d= 4000m) Global-Local System Direction Cosines

	$\hat{x}_L$	$\hat{y}_L$	$\hat{z}_L$
$\hat{x}_G$	1 - 1.92477e-7	3.9659e-7	-0.00062045
$\hat{y}_G$	3.9659e-7	1 - 2.04288e-7	0.00063920
$\hat{z}_G$	0.00062045	-0.00063920	1 - 3.9677e-7

Table 13: Hanford X Mid-Station (d = 2000m) Global-Local System Direction Cosines

	$\hat{x}_L$	$\hat{y}_L$	$\hat{z}_L$
$\hat{x}_G$	1 - 4.6765e-8	3.6722e-9	-0.000305827
$\hat{y}_G$	3.6722e-9	1 - 7.2090e-11	0.0000120075
$\hat{z}_G$	0.000305827	-0.0000120075	1 - 4.6837e-8

Table 14: Hanford Y Mid-Station (d = 2000m) Global-Local System Direction Cosines

	$\hat{x}_L$	$\hat{y}_L$	$\hat{z}_L$
$\hat{x}_G$	1 - 1.92182e-7	2.02012e-7	-0.00061997
$\hat{y}_G$	2.02012e-7	1 - 5.3086e-8	0.00032584
$\hat{z}_G$	0.00061997	-0.00032584	1 - 2.45268e-7

3 LIVINGSTON SURVEY DATA

TBD

4 GRAPHICAL REPRESENTATIONS OF THE INTERFEROMETER PLANES FOR EACH SITE

Figure 5 presents graphical representations of the orientations of the interferometer planes at the two sites relative to a surface of constant elevation (referred to the vertex) from various points of view. A spherical earth was assumed in generating the pictures (deviations from geoid or ellipsoid do not affect results at the level of precision required).

Figure 5: Representation of the interferometer plane inclinations at the two LIGO sites.

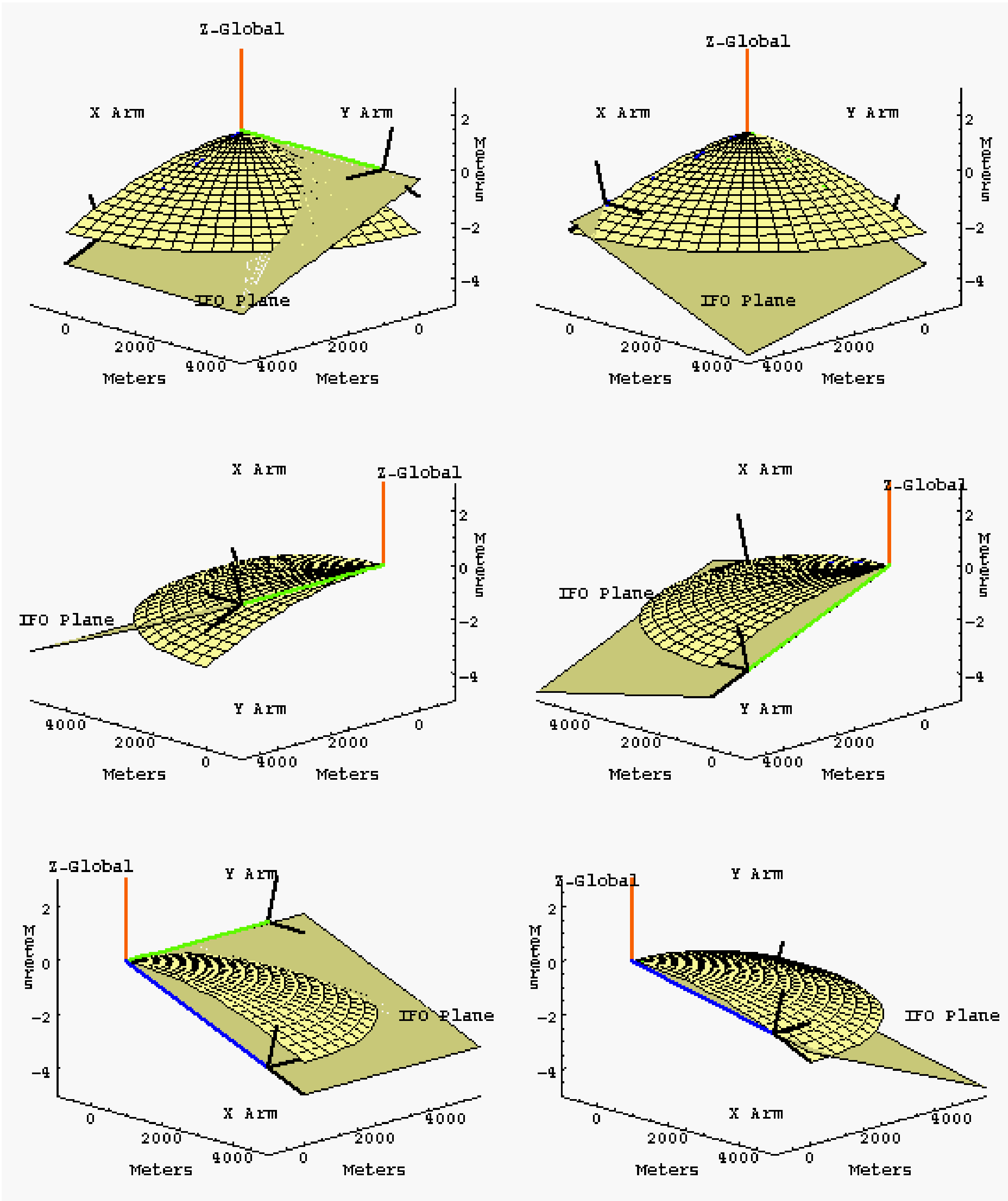

HANFORD, WA **LIVINGSTON, LA**